Generation of dust projectiles passing over an obstacle in the plasma sheath

Cătălin M. Ticoş,[1,a)] Daniel S. Stoica,[1] and Gian Luca Delzanno[2]
[1]*National Institute for Laser, Plasma and Radiation Physics, 077125 Bucharest, Romania*
[2]*Los Alamos National Laboratory, T-5 Applied Mathematics and Plasma Physics Group, Los Alamos, New Mexico 87545, USA*

(Received 29 March 2012; accepted 17 July 2012; published online 2 August 2012)

Dust projectiles were produced in a radio-frequency plasma by increasing 6-fold the radio-frequency power put into the discharge. The initial static dust particles were observed to gain speed while moving away from the confining region and escaped from the inter-electrode space on a ballistic-like trajectory. Single-grain dynamics simulations indicated that the dust particles were accelerated by changes induced in the sheath electric field profile. © *2012 American Institute of Physics*. [http://dx.doi.org/10.1063/1.4742169]

I. INTRODUCTION

Transport of dust grains in plasma is a subject of wide interest with far-reaching implications in topics as diverse as liquid dusty plasmas,[1] and lift-off and displacement of lunar dust.[2] Collective motion of dust grains has an influence on the operation of plasma processing reactors.[3] Moreover, understanding and control of dust transport are key problems for safe and reliable energy production in the next generation tokamaks.[4,5] Highly accelerated dust clouds could be used as a diagnostic tool for magnetic field mapping in fusion plasmas.[6,7]

Micrometer size grains can be easily trapped in the sheath of radio-frequency (rf) plasma produced between two parallel plate electrodes.[8] The microparticles acquire negative charges on their surface and are subjected to the electric force of the plasma sheath field which equilibrates the gravity force.[9] Confinement of the dust grains to a predetermined spatial region can be achieved by a cut in the electrode which deforms slightly the sheath and acts as an electrostatic "barrier" for the charged dust.

In this article, we report on a dust acceleration mechanism in the plasma sheath of a rf discharge. When the rf power was increased 6-fold, the dust grains initially at equilibrium in a plasma crystal were suddenly ejected out of the confining region and left the discharge. The process continued until few dust particles were left in the sheath. Furthermore, in this process the microparticles acquired a speed of a few cm/s over a short distance of ~ 5 mm, passing above the elevated part of the electrode. Great care has been taken to insure a good horizontal alignment of the rf driven electrode. The gas flow inside the chamber which could drag the particles during the observations has been suppressed by closing the valves of the vacuum pump and of the supplying gas tank. The influence of the rf power and gas pressure on dust particle trapping has been also reported elsewhere,[10] where it is briefly mentioned that dust particles escaped the confining zone at elevated rf power.

II. EXPERIMENTAL RESULTS

A. Electrode configuration

The experiment was performed in argon plasma obtained by applying a 13.56 MHz high-voltage signal on two horizontal electrodes placed 3 cm apart. The bottom electrode was driven by the rf signal and the top electrode was grounded and connected to the chamber wall, as shown in Fig. 1. The efficient transfer of rf power to the plasma was achieved by a matching network. The rf electrode was provided with a circular cut with 30 mm diameter and 1.5 mm depth. The electrode had therefore two distinct zones: a spatially extended hollow region and a slightly higher circular ring of 5 mm width. The plasma sheath followed the geometry of the electrode being approximately flat above most of the hollow region and slightly raised towards its edges.

Dust particles were released inside the plasma by shaking a small cylindrical container (≈ 1 cm^3) provided with a hole with 1 mm diameter. The cylinder was screwed at the end of a retractable long arm. During the experiment, the dispenser was pulled away from the electrodes to not perturb the plasma. Melamine formaldehyde particles with a

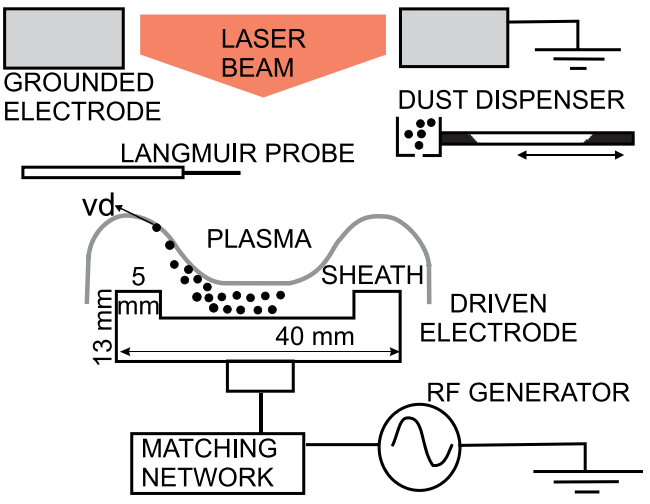

FIG. 1. Confined dust particles escape from the trapping region. The plasma sheath boundary is shown with grey line.

[a)]Author to whom correspondence should be addressed. Electronic mail: catalin.ticos@inflpr.ro.

diameter of 6.05 μm were trapped and confined above the hollow region of the rf electrode. They were illuminated with a vertical light sheet by passing the beam of a laser diode (15 mW at 680 nm) through a cylindrical lens. The dust particles were imaged with a high-speed camera Photron 1024 PCI from a side window of the vacuum chamber. The focusing optics consisted of a micro-Nikkor 60 mm f/2.8D lens, a teleconverter (3×), and a set of 3 spacers with total length of 68 mm. A red filter was put in front of the camera lens in order to cut out the plasma light. A calibration of the optical system produced images with an average resolution of 15 μm/pixel.

B. Dust motion tracking

Three different neutral gas pressures were set in the experiment: 110, 198, and 384 mTorr. At $p = 198$ and 384 mTorr, the stationary dust particles were forming a steady plasma crystal. For the lower pressure, i.e., 110 mTorr, some microparticles were oscillating about their equilibrium position.[11] In all three cases, the power injected into the plasma was increased from 3 W to 18 W in about 1 s, at constant pressure. The matching network was automatically tuned up to reflect less than 1 W of rf power. The plasma parameters have been measured with a Langmuir probe inserted midway between the electrodes. The most notable change during the rf power increase was a strong reduction in the dc self-bias of the rf driven electrode: V_{dc} had the largest drop from −65.5 V to −213 V at 110 mTorr, while at 384 mTorr it varied from −52 V to −159 V. In all 3 cases, the electron density n_e increased from $3.7 - 5.7 \times 10^{15}$ to $9.3 - 10.5 \times 10^{15}$ m^{-3}, while T_e was in the range 3.2 to 4.8 eV. The plasma potential increased slightly from 27.4 to 35.2 V. The probe measurements were carried out without dust at the same rf power levels as those set in the experiments with dust particles, i.e., 3 and 18 W, respectively.

The experiments started with plasma crystals with 10 to 15 horizontal layers. Dust projectiles were produced whenever the rf power was increased above a threshold of 5 W at pressures between 100 and 200 mTorr, and above 7 W for $p \gtrsim 290$ mTorr. At the rf power threshold, only a few particles escaped. At 18 W, the process turned into a "dust flow" and eventually most particles would escape. Interestingly, above 400 mTorr detrapping of the dust particles was not observed, regardless of the rf power level. In spite of sheath modification, only a vertical compression of the crystal width with about 20% was produced. In the pressure range of the experiment, the sheath width varied as indicated by the position of the dust particles; however, the most notable effect on the observed phenomenon was the change in the sheath curvature during the rf power increase, especially above the ridge zone and this was visible with the naked eye.

Three distinct phases could be identified in the dust dynamics during the rf power increase. In the first phase, the initial plasma crystal shown in Fig. 2(a) was vertically compressed. In the second phase, the whole plasma crystal slowly drifted horizontally towards the limit of the confining region as shown in Fig. 2(b). The arrows of Fig. 2(b) indicate the direction of the drift in the two phases: The bottom dust particles moved up with ≈17 mm/s while the crystal tip was traveling at a slower pace, of 3.7 mm/s. The particles at the extremity of the crystal moved faster than the ones found inside it which led to the formation of an elongated plasma crystal. In the third phase, the dust particles situated at the very edge of the confining region, slowly drifted away from the dust cloud, as shown in Figs. 3(a)–3(c), creating a dust stream. The moving particles passed above the ring zone of the electrode found ahead of them on a ballistic-like trajectory as seen in Figs. 3(b) and 3(c), during which they got accelerated. At the end of their trajectory, the particles left the inter-electrode region and fell on the chamber wall.

In the recorded frames, the instantaneous position of a particle is given by $(x(t), y(t))$. Both x and y are measured relative to the origin of axes shown in Fig. 3(a), i.e., the edge of the confining zone. The motion of a dust particle was tracked from its rest position until it disappeared from the viewing area. The measured dust trajectories presented in Fig. 4(a) are almost parabolic. The initial equilibrium height as well as the subsequent particle motion is pressure dependent, as seen in Figs. 4(a) to 4(c). The peak of each trajectory is $\Delta y \approx 0.5$ mm above the starting point and it is reached at $x \approx 3$ mm, slightly farther than the middle of the electrode ring zone ($x = 2.5$ mm).

The speed of the ballistic dust particles was measured by employing the time of flight technique. The exposure time in the recorded images is $t_{exp} = 4$ ms while the frame rate is 250 frames/s. The instantaneous speed is given by $v = (v_x^2 + v_y^2)^{1/2}$, with $v_x = \delta x / t_{exp}$, $v_y = \delta y / t_{exp}$, and δx and δy are the changes in the particle's coordinates in consecutive frames. The evolution of particles speed in time is

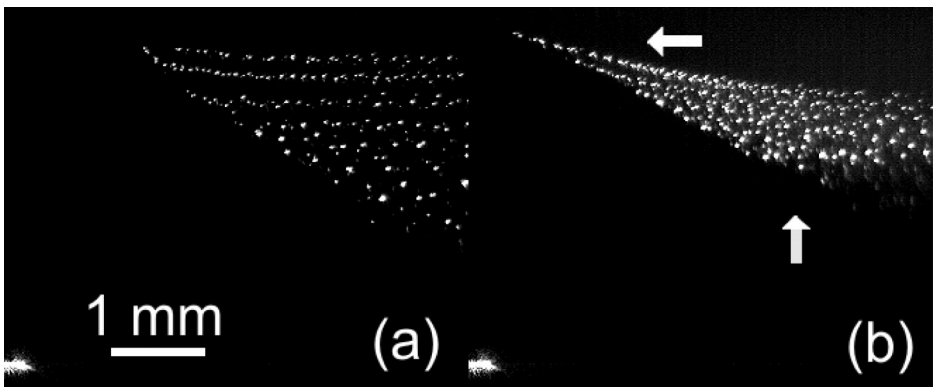

FIG. 2. (a) Stable crystal at P = 384 mTorr and 3 W; (b) vertically compressed and elongated crystal at ≈9 W drifting towards the edge of the confining region. The bright spot at the bottom of each image is the tip of the electrode.

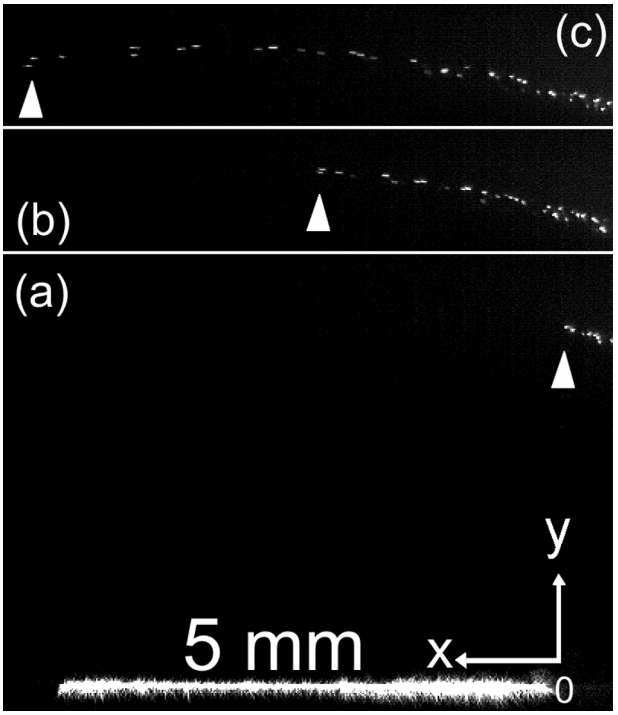

FIG. 3. Stream of dust particles (marked with an arrow) above the electrode illuminated with laser; (b) and (c) were recorded 236 ms and 360 ms after (a), respectively.

plotted in Fig. 4(b). At the highest pressure a particle attains about 3.5 cm/s, while at the other two pressures the maximum speed increases to 5.5 and 8 cm/s, respectively. The duration of the measured trajectory is longer at higher pressure ($\approx$0.42 s at 384 mTorr), compared to $\approx$ 0.25 s at 110 mTorr. Also, it appears that a particle climbs up slowly into the sheath for about 75% of its flight duration. After reaching the peak height, the particle moves a few times faster on its descending path.

A quadratic least-square fit of the type $v_{fit} = \alpha(t-\beta)^2$ approximates well the variation with time of a particle's speed. The coefficient α increases with decreasing gas pressure: $\alpha = 0.094, 1.029$, and $2.989\ \mathrm{m/s^3}$ in the 3 cases of Fig. 4, while β is $\simeq 0.1$ ms. The dust acceleration is easily deduced from the fit function: $a_{fit} = 2\alpha(t-\beta)$. Dust acceleration and therefore the force acting on a particle are not constant in time, but rather vary linearly. In Fig. 4(c), there is almost one order of magnitude difference between the slopes of a_{fit} corresponding to the extremes of gas pressures.

III. PARTICLE DYNAMICS SIMULATIONS IN THE SHEATH

A. Sheath model

In order to gain theoretical understanding of the reasons for the generation of the dust projectiles, dust motion in the sheath near the non-planar electrode has been studied using single-grain dynamics simulations. The sheath model consists of the continuity and momentum equations for the ions and Boltzmann electrons coupled with Poisson's equation:

$$\frac{\partial n_i}{\partial t} + \nabla \cdot (n_i \mathbf{V}) = 0, \tag{1}$$

$$\frac{\partial \mathbf{V}}{\partial t} + (\mathbf{V} \cdot \nabla)\mathbf{V} = -\nabla\phi, \tag{2}$$

$$\nabla^2 \phi = \exp(\phi) - n_i, \tag{3}$$

where n_i is the ion density, $\mathbf{V}$ is the ion velocity field, ϕ is the electrostatic potential, and $\mathbf{E} = -\nabla\phi$ is the electric field. The fields in Eqs. (1)–(3) are time-averaged over a rf cycle. In the model, we consider an argon plasma with bulk density $n_0 = 10^{16}\ \mathrm{m^{-3}}$, $T_e = 5$ eV, and $T_i = 0.1$ eV, giving an electron Debye length $\lambda_{De} \sim 0.2$ mm and sound speed $C_s \sim 3.5$ km/s. The following normalization applies: lengths to λ_{De}, $\mathbf{V}$ to $C_s = \sqrt{T_e/m_i}$ where m_i is the ion mass; n to n_0, ϕ to $e\phi/T_e$ ($e = 1.6 \times 10^{-19}$ C), time to C_s/λ_{De}, and E to $e\lambda_{De}/T_e$.

We note that the presence of the shaped electrode implies that the problem is at least two-dimensional. Also, we have neglected the ion pressure term in Eq. (2) due to cold ions ($T_i \ll T_e$). It is worth noting that in a rf discharge the ions move only in response to the time-averaged potential while the electrons respond to the instantaneous rf potential.[12] Here, we have instead used a Boltzmann relation for the electron density in order to focus exclusively on the effect of the shaped electrode on the sheath. Similarly, in this paper we only model the sheath near the electrode,

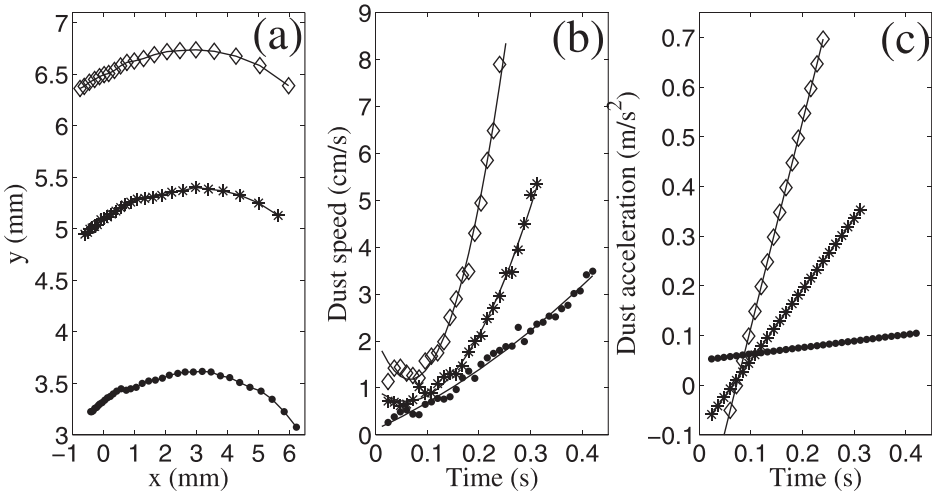

FIG. 4. (a) Measured dust trajectories at 110 (diamonds), 198 (stars), and 384 mTorr (dots); corresponding dust speed in (b) and accelerations in (c) of particles with $m_d = 1.75 \times 10^{-13}$ kg. Quadratic and linear fits (line) in (b) and (c), respectively.

unlike Sheridan,[13] who considered a two-dimensional cylindrical sheath model including an expanding presheath to study radial dust oscillations over a flat electrode with a confining ring. The details of the sheath-presheath transition should not change our results qualitatively, as long as the dust particles motion is away from the transition region.

Equations (1)–(3) are solved numerically on a two-dimensional domain with extension $L_x = 100$ and $L_y = 50$, in terms of λ_{De}. The domain is T-shaped and conforms to the surface of the electrode. The non-planarity of the electrode is characterized by two square tips of length $L_{\rm el}$ ($L_{\rm el} = 9$ at its edges). As boundary conditions, we use periodicity of the fields at $x = 0, L_x$, while at $y = L_y$ we prescribe $n_i = 1$, $V_y = -1$, $V_x = 0$, and $\phi = 0$ which correspond to an unperturbed plasma far away from the electrode with ions entering the sheath with a sonic velocity perpendicular to the electrode.[12] At the bottom of the domain, only the potential ϕ needs to be prescribed: $\phi = \phi_0$, with ϕ_0 the electrode potential.

Figure 5 shows the lines of the sheath profile ϕ and field V_x obtained at steady state with the electrode potential fixed at $\phi_0 = -30$, to match the experimental plasma potential and electrode voltage at 110 mTorr. The profile ϕ is symmetric relative to $x = L_x/2$. For a planar electrode (i.e., no tips) V_y becomes supersonic, $V_y(y = 0) \approx -7.8$, while $V_x = 0$ everywhere in the domain, and the ion density decreases to $n_i(y = 0) \approx 0.1$ due to flux conservation. In our case, the region near the center of symmetry does not feel the presence of the electrode tips such that the profiles match those of the planar electrode. However, at the electrode tip ($x \in [0, L_{\rm el}]$, and $y = L_{\rm el}$) the profiles V_y and n_i still reach the same values obtained for the planar case. A velocity field V_x parallel to the electrode is created in the vicinity of the tip. The magnitude of V_x is comparable to that of V_y, with the maximum $V_x \approx 4.3$, which means that ions have an horizontal directed motion inside the sheath.

B. Equation of motion for a dust particle

Dust motion is studied in the sheath above the non-planar electrode. The dust particles are treated as test particles which do not perturb the sheath. Dust transport is modeled using the equation of motion $d\mathbf{x}_d/dt = \mathbf{v}_d$ and $m_d d\mathbf{v}_d/dt = \sum_\alpha \mathbf{F}_\alpha$ with $\mathbf{x}_d$ ($\mathbf{v}_d$) the dust position (velocity), m_d the dust mass, and $\mathbf{F}_\alpha$ the forces acting on the dust. The following forces are considered: gravity $\mathbf{F}_g = -m_d g \mathbf{e}_y$ (with $g = 10\,{\rm m/s^2}$ and $\mathbf{e}_y$ the unit vector along y); ion drag,[9] $\mathbf{F}_{id} = 10\pi r_d^2 m_i n_i(\mathbf{x}_d) v_{thi}[\mathbf{V}(\mathbf{x}_d) - \mathbf{v}_d]$ (with r_d the dust radius and $v_{thi} = \sqrt{T_i/m_i}$ the ion thermal speed), the electrostatic force, $\mathbf{F}_E = Q_d \mathbf{E}(\mathbf{x}_d)$ (with $Q_d(\mathbf{x_d})$ the dust charge), and the neutral drag force $\mathbf{F}_{nd} = 2.67\sqrt{2\pi} r_d^2 m_n n_n v_{thn} \sqrt{1 + 9\pi s^2/64}\,(\mathbf{v}_n - \mathbf{v}_d)$,[14] where m_n, n_n, v_{thn}, and $\mathbf{v}_n$ are, respectively, the mass, density, thermal, and mean velocity of the neutrals and $s = |\mathbf{v}_d - \mathbf{v}_n|/\sqrt{2 v_{thn}}$. Furthermore, the equations for dust motion are coupled to the dust charging equation obtained from the orbital motion limited (OML) theory.[9] We notice that the ion drag and electrostatic forces require knowledge of the sheath profiles interpolated at the dust particle position. In the steady state sheath (such as in Fig. 5), a dust grain has its equilibrium position in the plane of symmetry of the system, $x = L_x/2$, at a height above the electrode where the electrostatic force balances the gravitational force. Introducing a dust grain at any other location in the sheath results in dust motion, which remains however confined in the x direction due to the sheath electric field E_x generated by the shaped electrode. The dust grain turns around and moves away from the electrode tip, towards the central region where the horizontal electrostatic force decreases. Radial oscillations in a parabolic confining potential well created by an electrode with similar geometry have been studied in Ref. 13.

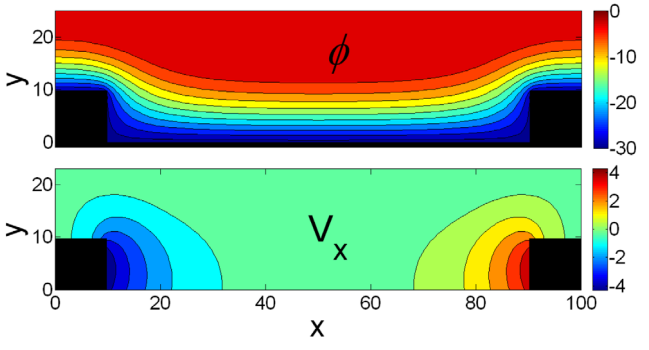

FIG. 5. Steady state potential distribution ϕ and ion speed V_x near the rf electrode, from models (1)–(3) and with electrode potential $\phi_0 = -30$.

C. Results

We investigated the sheath field profiles and dust transport when the rf power was increased. The power increase was modeled by setting a linear function in time for the electrode potential: $\phi_0(\tau) = \phi_A + (\phi_B - \phi_A)\tau$, for $\tau \in [0, 1]$ s and $\phi_0(\tau) = \phi_B$ for $\tau > 1$ s, where $\phi_A = -30$ and $\phi_B = -50$. Qualitatively, the time-dependent sheath profiles obtained by (1)–(3) are topologically similar to those for the stationary case ($\tau = 0$). The main difference is in the magnitude of the profiles: for instance at $\tau \geq 1$, $V_y(L_x/2, 0) \approx -8.5$, while the electric field change is more sizeable, $\max|E_y| \approx 8$ and $\max|E_x| \approx 6.3$ compared to ≈ 5.5 and ≈ 4.4, respectively, before the rf power increase.

Simulations of dust motion in the time-dependent sheath field were carried out for individual test particles located at $x_d = 20$ and $y_d \in [6, 20]$. We considered the case with neutral pressure $p_n = 110\,{\rm mTorr}$ (the neutral temperature is $T_n = 0.025$ eV) and assumed that the average speed of the neutrals is zero. A constant force $\mathbf{F}_{crys}$ that holds the dust particle in equilibrium at the beginning of the simulation was added. It essentially replaced the effect of the other dust particles that would be present in a steady state crystal like the one in the experiment, compensating for the horizontal confining force. The dust trajectories are presented in Fig. 6. The dust particles with $y_d \lesssim 14$ fall on the electrode. This is not surprising considering that particles very close to the electrode tend to charge positively and are attracted towards it. However, for $y_d > 14$ the particles are ejected from the sheath and pass over the tip of the electrode with a parabolic motion similar to that of the experiments. A particle initially at $x_d = 20$ and $y_d = 18$ starts to acquire a very small vertical

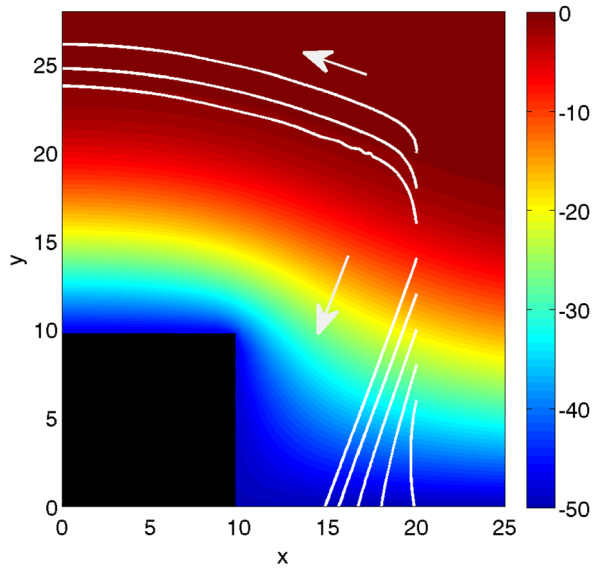

FIG. 6. Trajectories of dust particles moving past the electrode or falling near its tip, depending on initial height, obtained from single-grain dynamics simulations. Contours of the potential at $\tau = 1$ s are superimposed.

velocity as the electrode potential is decreased, and moves away from the electrode. At $\tau = 0.5$ s, $y_d \approx 19.4$. During this ascending motion, the particle net force in the x direction is approximately zero and the electric field E_x at the particle position remains roughly constant. Consequently, the particle does not move much along x: $x_d \approx 19.5$. At about $\tau \sim 0.85$ s, $E_x(\mathbf{x}_d)$ starts decreasing because E_x is localized near the electrode tip but the grain is moving away from it ($y_d \approx 21.0$) and the force balance in the x direction is lost. $\mathbf{F}_{\mathbf{crys}}$ pushes the dust particle over the electrode tip and outside the domain. It is interesting to note that, although the non-planarity of the electrode gives rise to a sizeable V_x near the tip of the electrodes, within our model the ion drag $\propto \mathbf{V}$ is negligible in the parameter regime considered and our results indicate that the generation of the dust projectiles can be due to the electrostatic force. However, we note that, while qualitative, our results are strongly dependent on the details of the (constant) force $\mathbf{F}_{\mathbf{crys}}$ that characterizes the effect of other dust grains in the crystal on the test dust particle. In a realistic situation, $\mathbf{F}_{\mathbf{crys}}$ will vary in space and time non-trivially as the dust particles adjust to the dynamically changing sheath. Future work will focus on modeling $\mathbf{F}_{\mathbf{crys}}$ more realistically by studying the interaction of a system of dust grains in the time-dependent sheath.

IV. CONCLUSIONS

We have presented a new mechanism for acceleration and transport of dust grains outside the trapping region in the plasma sheath over an irregular electrode. Single-grain dynamics simulations in the time-dependent sheath have suggested the important role played by the electrostatic force in this technique: The shaped electrode and the power increase induced changes in the curvature and strength of the sheath electric field which, combined with the repulsive force of other nearby dust grains, accelerated the dust grains located near the edge of the trapping region. The empty void left behind them was then filled by nearby dust grains drifting towards the electrode edge and the process continued giving rise to a dust stream. This technique could be used for efficient transport and eventual removal of dust grains trapped in the plasma sheath. Moreover, the idea of induced dust motion above a surface driven by the sheath electric force could be exploited outside typical laboratory rf discharges,[15] e.g., in magnetic fusion applications where control of dust transport in the magnetized sheath of the divertor is desirable.[5]

ACKNOWLEDGMENTS

C.M.T. acknowledges support from the National Authority for Scientific Research (ANCS) under program Nucleu-LAPLAS 2012. G.L.D. wishes to thank Xianzhu Tang and Enrico Camporeale for discussions. Part of this research was performed under the auspices of the NNSA of the U.S. DOE by LANL, operated by LANS LLC under Contract DE-AC52-06NA25396.

[1]G. E. Morfill, M. Rubin-Zuzic, H. Rothermel, A. V. Ivlev, B. A. Klumov, H. M. Thomas, and U. Konopka, Phys. Rev. Lett. **92**, 175004 (2004).
[2]X. Wang, M. Horányi, and S. Robertson, J. Geophys. Res. **115**, A11102 (2010).
[3]L. Couëdel, M. Mikikian, A. A. Samarian, and L. Boufendi, Phys. Plasmas **17**, 083705 (2010).
[4]S. I. Krasheninnikov, A. Yu. Pigarov, R. D. Smirnov, M. Rosenberg, Y. Tanaka, D. J. Benson, T. K. Soboleva, T. D. Rognlien, D. A. Mendis, B. D. Bray, D. L. Rudakov, J. H. Yu, W. P. West, A. L. Roquemore, C. H. Skinner, J. L. Terry, B. Lipschultz, A. Bader, R. S. Granetz, C. S. Pitcher, N. Ohno, S. Takamura, S. Masuzaki, N. Ashikawa, M. Shiratani, M. Tokitani, R. Kumazawa, N. Asakura, T. Nakano, A. M. Litnovsky, R. Maqueda, and LHD Experimental Group, Plasma Phys. Controlled Fusion **50**, 124054 (2008).
[5]X. Z. Tang and G. L. Delzanno, J. Fusion Energy **29**, 407 (2010).
[6]Z. Wang and G. A. Wurden, Rev. Sci. Instrum. **74**, 1887 (2003).
[7]C. M. Ticos, Z. Wang, G. A. Wurden, J. L. Kline, D. S. Montgomery, L. A. Dorf, and P. K. Shukla, Phys. Rev. Lett. **100**, 155002 (2008).
[8]G. S. Selwyn, J. E. Heidenreich, and K. L. Haller, Appl. Phys. Lett. **57**, 1876 (1990).
[9]P. K. Shukla and B. Eliasson, Rev. Mod. Phys. **81**, 25 (2009).
[10]J. B. Pieper, J. Goree, and R. A. Quinn, J. Vac. Sci. Technol. A **14**, 519 (1996).
[11]A. A. Samarian, B. W. James, S. V. Vladimirov, and N. F. Cramer, Phys. Rev. E **64**, 025402(R) (2001).
[12]M. A. Lieberman and A. J. Lichtenberg, *Principles of Plasma Discharges and Materials Processing* (Wiley, New York, 1994).
[13]T. E. Sheridan, J. Appl. Phys. **98**, 023302 (2005).
[14]B. T. Draine and E. E. Salpeter, Astrophys. J. **231**, 77 (1979).
[15]Y.-F. Li, U. Konopka, K. Jiang, T. Shimizu, H. Höfner, H. M. Thomas, and G. E. Morfill, Appl. Phys. Lett. **94**, 081502 (2009).